Supplemental Materials

Monoacylglycerol lipase exerts bidirectional control over endocannabinoid and fatty acid pathways to support prostate cancer pathogenesis

Daniel K. Nomura[1*], Donald P. Lombardi[1], Jae Won Chang, Sherry Niessen, Anna M. Ward, Jonathan Z. Long, Heather H. Hoover, and Benjamin F. Cravatt*

[1] these authors contributed equally to the work

*correspondence to cravatt@scripps.edu and dnomura@scripps.edu

Supplemental Methods

Lipidomic analysis of Prostate Cancer Cells

Lipidomic analyses were performed as previously described (Nomura et al., 2010). Lipid measurements were conducted in cancer cells grown in serum-free media for 4 hrs to minimize the contribution of serum-derived lipids to the cellular profiles. Cancer cells (1×10^6 cells/6 cm dish, 80 % confluency) were washed with twice with phosphate buffer saline (PBS), isolated by centrifugation at 1,400 x g, and dounce-homogenized in 4 ml of a 2:1:1 mixture of chloroform:methanol:50 mM Tris buffer (pH 8.0) with the inclusion of internal standards C12:0 MAGE (10 nmol) and C15:0 FFA (10 nmol). Organic and aqueous layers were separated by centrifugation and the organic layer was collected. The aqueous layer was acidified by adding 0.2 % formic acid, followed by the addition of 2 ml chloroform. The mixture was vortexed, and the organic layers were combined, dried down under N_2 and dissolved in 100 µl chloroform, of which 30 µl was analyzed by LC-MS.

Untargeted LC-MS analysis was performed by using an Agilent 6520 Accurate Mass QTOF LC/MS instrument. LC separation was achieved with a Gemini reverse-phase C18 column (50 mm x 4.6 mm with 5 µm diameter particles) from Phenomonex. Mobile phase A was composed of a 95:5 ratio of water:methanol, and mobile phase B consisting of a 60:35:5 ratio of 2-propanol, methanol, and water. Solvent modifiers 0.1% formic acid and 0.1% ammonium hydroxide were used to assist ion formation in positive and negative ionization modes, respectively. The flow rate for each run started at 0.1 ml/min for 5 min, to alleviate backpressure associated with injecting chloroform. The gradient started at 0% B and increased linearly to 100% B over the course of 45 min with a flow rate of 0.4 ml/min, followed by an isocratic gradient of 100% B for 17 min at 0.5 ml/min before equilibrating for 8 min at 0% B with a flow rate of 0.5 ml/min. MS analysis was performed with an electrospray ionization (ESI) source. The

capillary voltage was set to 4.0 kV, and the fragmentor voltage was set to 100 V. The drying gas temperature was 350^{o}C, the drying gas flow rate was 11 L/min, and the nebulizer pressure was 45 psi. Untargeted data were collected using a mass range of 200–1200 Da and were exported as common data format (.mzdata.xml) files for computational analysis. Differentially expressed metabolites between sample pairs were identified by using the XCMS analyte profiling software (http://metlin/download), which aligns and quantifies the relative signal intensities of mass peaks from multiple LC-MS traces (Smith et al., 2006). Significant inhibitor, shMAGL or JZL184-sensitive peak changes were confirmed by manual quantification by using the area under the peak normalized to the internal standards (C12 MAGE for positive mode and C15:0 FFA for negative mode). Additionally, 46 representative lipids were also extracted out of untargeted datasets and quantified **(Table S2)**. The identity of these lipids were confirmed by coelution and mass accuracy of <10 ppm of the endogenous metabolite with its corresponding standard. Lipids were quantified by measuring the area under the peak in comparison to an external standard curve of the corresponding metabolite standards to a set concentration of internal standards.

Select MAG and LPA lipid species were also quantitated by an Agilent G6410B QQQ instrument for confirmation of data obtained from QTOF-LC/MS analysis. Values obtained were within 5 % of quantitation obtained by QTOF-LC/MS analysis. LC separation was achieved as above but with a shorter LC program. The flow rate for each run started at 0.1 ml/min with 0% B. At 5 min, the solvent was immediately changed to 60% B with a flow rate of 0.4 ml/min and increased linearly to 100% B over 10 min. This was followed by an isocratic gradient of 100% B for 5 min at 0.5 ml/min before equilibrating for 3 min at 0% B at 0.5 ml/min (23 min total per sample). The following MS parameters were used to measure the indicated metabolites (precursor ion, product ion, collision energy in V, ionization): C20:4 MAG (379, 287, 8, positive), C18:1 MAG (357, 265, 8, positive), C16:0 MAG (331, 239, 8, positive), C12:0 MAGE (261, 261, 0, positive),

pentadecanoic acid (241, 241, 0, negative), C16:0 LPA (409, 79, 40, negative), C18:0 LPA (437, 79, 40, negative), C18:1 LPA (435, 79, 40, negative). MS analysis was performed with an electrospray ionization (ESI) source. The dwell time for each lipid was set to 60 ms. The capillary was set to 4 kV, the fragmentor was set to 100 V, and the delta EMV was set to +300. The drying gas temperature was 350°C, the drying gas flow rate was 11 L/min, and the nebulizer pressure was 35 psi.

Supplemental Figure and Table Legends

Table S1. Proteomic data obtained from ABPP-MudPIT analysis. Values are expressed in spectral counts. **Tab 1** includes all proteomic data obtained from ABPP-MudPIT. **Tab 2** contains serine hydrolase activities that were filtered for enzymes that displayed: 1) > 10-fold higher spectral counts in FP-biotin-treated proteomes compared to "no-probe" (NP) control proteomes (samples not subjected to FP-biotin labeling) for at least one of the cancer cell lines examined, and 2) an average of ≥ 6 spectral counts for at least one of the cancer cell lines examined. Data are shown from individual replicates for 3-4 independent experiments per cell line for FP-biotin labeled proteomes. Related to **Table 1**.

Table S2. Lipid quantitation in prostate cancer cells. For JZL184 treatments, 1 x 10^6 cells (~80 % confluence) were serum-starved in serum-free media for 4 h with DMSO or JZL184 (1 μM) (0.1 % final DMSO concentration), before isolation of cells for lipidomic analysis. For shMAGL groups, cells were serum-starved as above for 4 h, without any treatments, before cells were isolated. All values are expressed in pmoles of metabolites/10^6 cells. Metabolite abbreviations are as follows: MAG, monoacylglycerol; MAGE, monoalkylglycerol ether; LPC,

lysophosphatidylcholine; LPE, lysophosphatidyl ethanolamine; PAF, platelet activating factor; PC, phosphatidylcholine; PE, phosphatidylethanolamine; LPA, lysophosphatidic acid; PA, phosphatidic acid; FFA, free fatty acid; S1P, sphingosine-1-phosphate; PS, phosphatidylserine. ND denotes "not determined" or metabolites which were not measured. Related to **Figure 1** and **Figure 2.**

Table S3. Microarray analysis of aggressive versus non-aggressive cancer cell lines. mRNA transcript levels were compared between aggressive (231MFP, SKOV3, C8161, PC3 and DU145) versus non-aggressive (MCF7, OVCAR3, MUM2C, LNCaP) cells from breast, ovarian, melanoma, and prostate cancers, respectively using Affymetrix HU133 Plus 2.0 microarrays **(Tab 1)**. Data were then filtered for genes that were commonly up- or down-regulated (>3-fold) in at least 4 out of the 5 pairs of aggressive versus non-aggressive cancer cell lines **(Tabs 2 and 3)**. Among these genes, we found that aggressive cancer cells were enriched in genes that have been associated with epithelial-to-mesenchymal transition (EMT) and cancer stem cell (CSC) markers **(Tabs 4 and 5)**. We also find that there are several other commonly dysregulated metabolic enzymes that correlate with cancer cell aggressiveness beyond MAGL **(Tabs 6 and 7)**. Related to **Figure 5**.

Figure S1. MAGL ablation regulates monoacylglycerol and free fatty acid metabolism and cancer pathogenicity in prostate cancer cells. (A,B) Inhibition of MAGL (JZL184 1 μM, 4 h in situ) raises MAG **(A)** and lowers FFA **(B)** levels in DU145 cells. **(C)** MAGL blockade by JZL184 also reduces lysophosphatidic acid (LPA) and phosphatidic acid (PA) levels in DU145. **(D,E,F)** Blockade of MAGL (JZL184 1 μM, 4 h in situ) impairs DU145 cancer cell migration **(D)**, invasion **(E)**, and serum-free cell survival **(F).** JZL184 was pretreated in serum-free media for 4

h before migration (24 h migration time), invasion (24 h invasion time), and cell survival (0, 1, 2, and 3 day) assays. For DU145 migration, representative fields of migrated cells are shown at 200 x magnification. **(G)** Lipidomic profile of JZL184-treatment (4 days, 1 μM) versus DMSO treatment in PC3 cells. **(H)** Diagram of metabolic pathways that MAGL regulates in prostate cancer cells. Under acute MAGL blockade, MAGs get shunted to LPC, while the fatty acid and downstream LPA, PA, and LPE fatty acid products are depleted. Under chronic MAGL blockade, LPC elevations are no longer evident, possibly due to incorporation into larger phosphatidyl choline pools. In non-aggressive LNCaP cells, we find that CPT1 expression is significantly higher compared to aggressive cancer cells, possibly indicating that fatty acids may be getting shunted into oxidative pathways. Significance expressed as *p<0.05, **p<0.01 for JZL184-treated versus DMSO-treated control groups. Data are presented as means ± standard error of the mean (SEM); n=4-5/group. Related to **Figure 1, Figure 2,** and **Figure 3.**

Figure S2. Genetic knockdown of MAGL Impairs PC3 Tumor Xenograft Growth. 2 x 10^6 PC3 parental, shControl, or shMAGL cells were injected into the flank of C.B17 SCID mice and growth of the tumors was measured every 3 days with calipers. Significance is expressed as **p<0.01 for shMAGL tumors versus shControl tumors. Data are presented as means ± standard error of the mean (SEM); n=6-8/group. Related to **Figure 3**.

Figure S3. Differential Effects of JZL184 in Scid versus Nude Mice. (A) JZL184 treatment (40 mg/kg, oral gavage, once daily in 4 μl/g mouse PEG300) significantly reduces PC3 tumor xenograft growth in scid mice but not in nude mice. **(B)** MAG hydrolytic activity analysis in PC3 tumor homogenate (left panel) shows that nude mice are less sensitive to JZL184 compared to scid mice at both 4 and 24 h after final JZL184 treatment (after 37 daily JZL184 treatments). Under acute 4 h and 24 h treatment, MAG hydrolytic activity analysis in brain and liver unsoluble

proteomes shows that nude mice are less sensitive to JZL184 inhibition of MAGL compared to scid mice. Significance expressed as **p<0.01 for JZL184-treatment groups versus corresponding vehicle groups, ## p<0.01 for JZL184-treatment groups in nude mice versus the matching time-point JZL184-treatment groups in scid mice. Data are presented as means ± standard error of the mean (SEM); n=6 mice/group. Related to **Figure 3**.

Figure S4. Effects of MAGL Overexpression and Knockdown in Prostate Cancer Cells. (A) MAGL was stably overexpressed (MAGL-OE) in the non-aggressive LNCaP cell line, confirmed by ABPP, by methods previously outlined (Nomura et al., 2010). EV corresponds to parental LNCaP cancer cells infected with empty vector. **(B, C)** MAGL overexpression does not alter FFA levels in LNCaP cells **(B)**, despite depletion of MAGs **(C)**. **(D)** MAGL overexpression does not alter the levels of several phospholipid species such as lysophosphatidyl ethanolamine (LPE), phosphatidic acid (PA), lysophosphatidyl choline (LPC), phosphatidyl choline (PC), and phosphatidyl ethanolamine (PE) species. **(E)** MAGL overexpression does not alter LNCaP migration over a 24 h time period. **(F)** Carnitine palmitoyltransferase 1 (CPT1) expression is higher in the non-aggressive LNCaP cell line compared to the aggressive PC3 and DU145 cells (data from gene expression data in **Figure 5, Table S3)**.**(G)** PC3 migration is impaired by treatment with the endogenous cannabinoid receptor ligand C20:4 MAG treatment (1 μM). Migratory defects conferred by MAGL knockdown are reversed upon CB1 antagonism (by rimonabant, RIM, 1 μM), but not by CB2 antagonism (by AM630, 1 μM). Pertussis toxin (PTX, 100 ng/ml) impairs basal PC3 migration. The partial rescue by FFA treatment (C16:0 FFA, 10 μM) of migratory defects conferred by MAGL knockdown is reversed by PTX treatment (100 ng/ml). **(H, I)** Invasion **(H)** and cell survival **(I)** defects conferred by MAGL knockdown is partially reversed by RIM (1 μM) or FFA (10 μM) treatment and fully reversed by dual treatment with RIM and FFA. All pharmacological agents were pre-treated in serum-free media with cells for 4 h before initiation of migration (5 h for PC3), invasion (24 h for PC3), or cell survival (3 days).

Cells were also re-treated with the pharmacological agents during the migration or invasion assays. *p<0.05, **p<0.01 for pharmacological treatment, MAGL-OE, or shMAGL groups versus EV or shControl groups. ## p<0.01 for pharmacological treatment of shControl or shMAGL groups versus shMAGL groups. Data are presented as means ± SEM. For **(B-E, G-H)**, n=4/group, for **(I)**, n=5/group. Related to **Figure 4.**

Table S4. Established literature precedence of genes enriched in aggressive cancer cells that are EMT/cancer stem cell markers. Genes listed below correspond to those listed in Figure 5B and Table S3 Tabs 4 and 5.

Gene	Reference
VIM	(Polyak and Weinberg, 2009)
ANXA1	(Maschler et al., 2010)
SFN	(Hunakova et al., 2009)
AXL	(Gjerdrum et al., 2010)
S100A4	(Okada et al., 1997)
TM4SF1	(Seo et al., 2007)
DKK1	(Matushansky et al., 2007)
CYR61	(Haque et al., 2011)
IGFBP3	(Natsuizaka et al., 2010)
TGFBI	(Polyak and Weinberg, 2009)
TACSTD2	(Ibragimova et al., 2010)
CD44	(Polyak and Weinberg, 2009)
PLAU	(Vuoriluoto et al., 2010)
PDGFC	(Patel et al., 2010)
CTGF	(Burns and Thomas, 2010)
LOXL2	(Polyak and Weinberg, 2009)
SMURF2	(Yang et al., 2010)
MET	(Ponzo et al., 2009)
HLA-G	(Selmani et al., 2009)
ETS1	(Lin et al., 2009)
F3	(Rak et al., 2008)
FOSL1	(Lemieux et al., 2009)
RAC2	(Sengupta et al., 2010)
LAMB3	(Polyak and Weinberg, 2009)
TGFBR2	(Polyak and Weinberg, 2009)
IGFBP4	(Natsuizaka et al., 2010)
TGM2	(Shao et al., 2009)
ZEB1	(Drake et al., 2009)
CXCL2	(Pelus and Fukuda, 2006)
LAMC2	(Drake et al., 2010)
PLAUR	(Jo et al., 2010)
LPAR1	(Pebay et al., 2007)
IFI16	(Yu et al., 2010)

PPARG	(Reka et al., 2010)
ITGA3	(Kurata et al., 2004)
SPTBN1	(Yao et al., 2010)
EGFR	(Beck et al., 2010)
BDNF	(Dudas et al., 2011)
GPR39	(Metsuyanim et al., 2009)
LOX	(Polyak and Weinberg, 2009)
GAS6	(Gjerdrum et al., 2010)

Figure S1

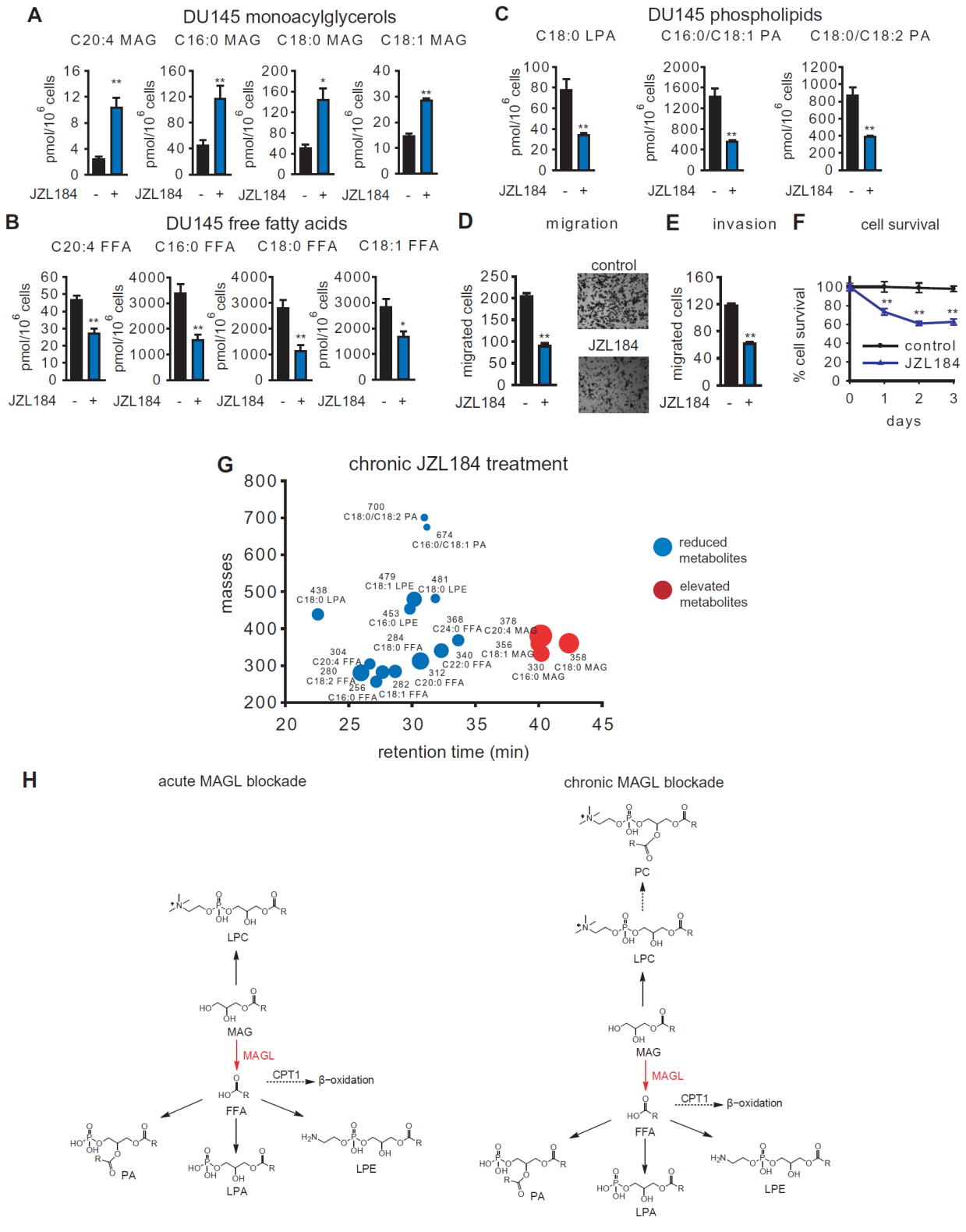
A
DU145 monoacylglycerols
C20:4 MAG
C16:0 MAG
C18:0 MAG
C18:1 MAG
pmol/10^6 cells
JZL184 - +
B
DU145 free fatty acids
C20:4 FFA
C16:0 FFA
C18:0 FFA
C18:1 FFA
C
DU145 phospholipids
C18:0 LPA
C16:0/C18:1 PA
C18:0/C18:2 PA
D
migration
migrated cells
control
JZL184
E
invasion
F
cell survival
% cell survival
control
JZL184
days
G
chronic JZL184 treatment
masses
retention time (min)
700 C18:0/C18:2 PA
674 C16:0/C18:1 PA
479 C18:1 LPE
481 C18:0 LPE
438 C18:0 LPA
453 C16:0 LPE
368 C24:0 FFA
378 C20:4 MAG
284 C18:0 FFA
356 C18:1 MAG
304 C20:4 FFA
340 C22:0 FFA
358 C18:0 MAG
280 C18:2 FFA
312 C20:0 FFA
330 C16:0 MAG
256 C16:0 FFA
282 C18:1 FFA
reduced metabolites
elevated metabolites
H
acute MAGL blockade
chronic MAGL blockade
LPC
MAG
MAGL
CPT1
β-oxidation
FFA
PA
LPA
LPE
PC

Figure S2

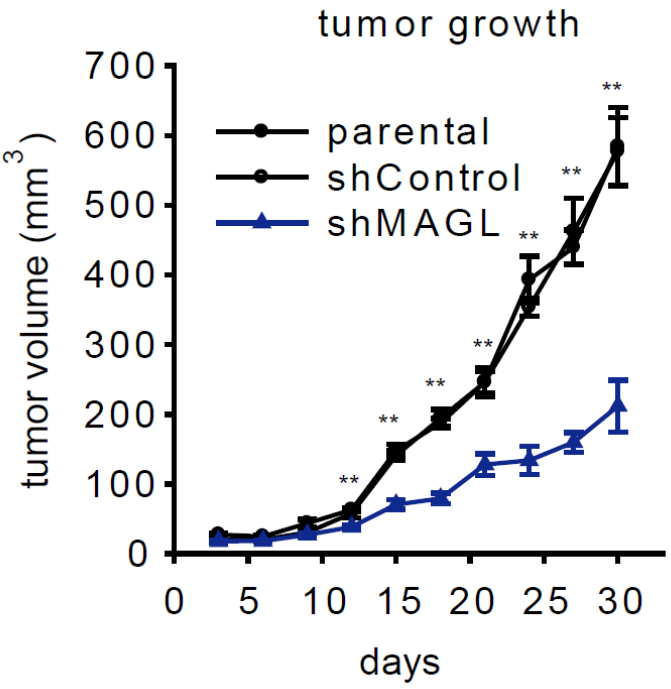
tumor growth
700
600
500
400
300
200
100
0
tumor volume (mm3)
parental
shControl
shMAGL
**
0
5
10
15
20
25
30
days

Figure S3

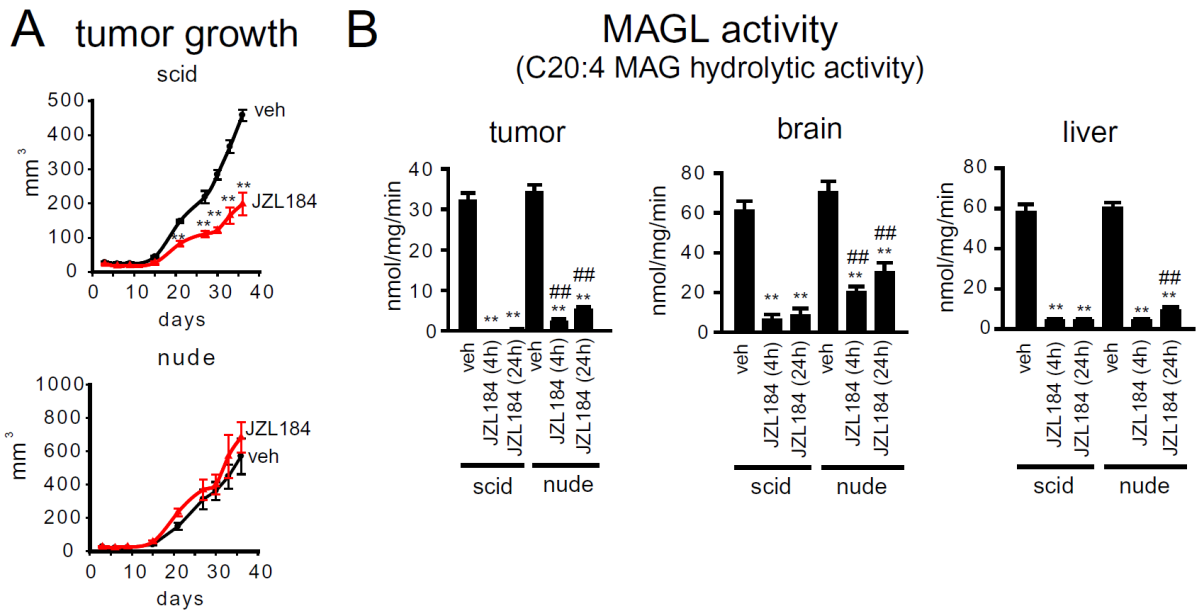
A tumor growth
scid
mm3
days
veh
JZL184
nude
JZL184
veh
B
MAGL activity
(C20:4 MAG hydrolytic activity)
tumor
brain
liver
nmol/mg/min
veh
JZL184 (4h)
JZL184 (24h)
scid
nude

Figure S4

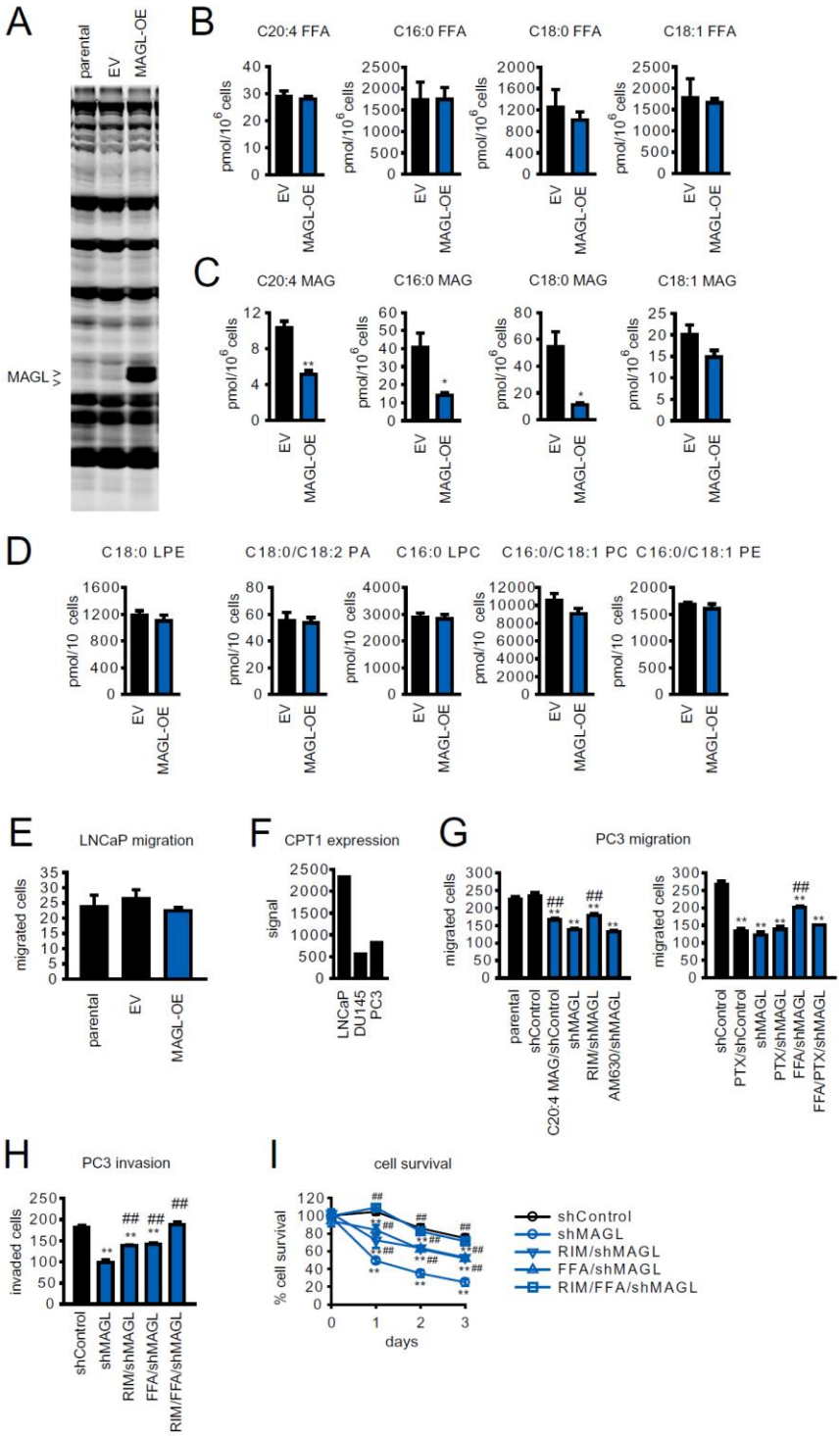
A
parental
EV
MAGL-OE
MAGL
B
C20:4 FFA
C16:0 FFA
C18:0 FFA
C18:1 FFA
pmol/10^6 cells
EV
MAGL-OE
C
C20:4 MAG
C16:0 MAG
C18:0 MAG
C18:1 MAG
D
C18:0 LPE
C18:0/C18:2 PA
C16:0 LPC
C16:0/C18:1 PC
C16:0/C18:1 PE
pmol/10 cells
E
LNCaP migration
migrated cells
parental
EV
MAGL-OE
F
CPT1 expression
signal
LNCaP
DU145
PC3
G
PC3 migration
migrated cells
parental
shControl
C20:4 MAG/shControl
shMAGL
RIM/shMAGL
AM630/shMAGL
shControl
PTX/shControl
shMAGL
PTX/shMAGL
FFA/shMAGL
FFA/PTX/shMAGL
H
PC3 invasion
invaded cells
shControl
shMAGL
RIM/shMAGL
FFA/shMAGL
RIM/FFA/shMAGL
I
cell survival
% cell survival
days
shControl
shMAGL
RIM/shMAGL
FFA/shMAGL
RIM/FFA/shMAGL

References

Beck, S., Jin, X., Sohn, Y.W., Kim, J.K., Kim, S.H., Yin, J., Pian, X., Kim, S.C., Nam, D.H., Choi, Y.J.*, et al.* (2010). Telomerase activity-independent function of TERT allows glioma cells to attain cancer stem cell characteristics by inducing EGFR expression. Mol Cells.

Burns, W.C., and Thomas, M.C. (2010). The molecular mediators of type 2 epithelial to mesenchymal transition (EMT) and their role in renal pathophysiology. Expert Rev Mol Med *12*, e17.

Drake, J.M., Barnes, J.M., Madsen, J.M., Domann, F.E., Stipp, C.S., and Henry, M.D. (2010). ZEB1 coordinately regulates laminin-332 and {beta}4 integrin expression altering the invasive phenotype of prostate cancer cells. J Biol Chem *285*, 33940-33948.

Drake, J.M., Strohbehn, G., Bair, T.B., Moreland, J.G., and Henry, M.D. (2009). ZEB1 enhances transendothelial migration and represses the epithelial phenotype of prostate cancer cells. Mol Biol Cell *20*, 2207-2217.

Dudas, J., Bitsche, M., Schartinger, V., Falkeis, C., Sprinzl, G.M., and Riechelmann, H. (2011). Fibroblasts produce brain-derived neurotrophic factor and induce mesenchymal transition of oral tumor cells. Oral Oncol *47*, 98-103.

Gjerdrum, C., Tiron, C., Hoiby, T., Stefansson, I., Haugen, H., Sandal, T., Collett, K., Li, S., McCormack, E., Gjertsen, B.T.*, et al.* (2010). Axl is an essential epithelial-to-mesenchymal transition-induced regulator of breast cancer metastasis and patient survival. Proc Natl Acad Sci U S A *107*, 1124-1129.

Haque, I., Mehta, S., Majumder, M., Dhar, K., De, A., McGregor, D., Van Veldhuizen, P.J., Banerjee, S.K., and Banerjee, S. (2011). Cyr61/CCN1 signaling is critical for epithelial-mesenchymal transition and stemness and promotes pancreatic carcinogenesis. Mol Cancer *10*, 8.

Hunakova, L., Sedlakova, O., Cholujova, D., Gronesova, P., Duraj, J., and Sedlak, J. (2009). Modulation of markers associated with aggressive phenotype in MDA-MB-231 breast carcinoma cells by sulforaphane. Neoplasma *56*, 548-556.

Ibragimova, I., Ibanez de Caceres, I., Hoffman, A.M., Potapova, A., Dulaimi, E., Al-Saleem, T., Hudes, G.R., Ochs, M.F., and Cairns, P. (2010). Global reactivation of epigenetically silenced genes in prostate cancer. Cancer Prev Res (Phila) *3*, 1084-1092.

Jo, M., Eastman, B.M., Webb, D.L., Stoletov, K., Klemke, R., and Gonias, S.L. (2010). Cell signaling by urokinase-type plasminogen activator receptor induces stem cell-like properties in breast cancer cells. Cancer Res *70*, 8948-8958.

Kurata, S., Okuyama, T., Osada, M., Watanabe, T., Tomimori, Y., Sato, S., Iwai, A., Tsuji, T., Ikawa, Y., and Katoh, I. (2004). p51/p63 Controls subunit alpha3 of the major epidermis integrin anchoring the stem cells to the niche. J Biol Chem *279*, 50069-50077.

Lemieux, E., Bergeron, S., Durand, V., Asselin, C., Saucier, C., and Rivard, N. (2009). Constitutively active MEK1 is sufficient to induce epithelial-to-mesenchymal transition in intestinal epithelial cells and to promote tumor invasion and metastasis. Int J Cancer *125*, 1575-1586.

Lin, J.C., Liao, S.K., Lee, E.H., Hung, M.S., Sayion, Y., Chen, H.C., Kang, C.C., Huang, L.S., and Cherng, J.M. (2009). Molecular events associated with epithelial to mesenchymal transition of nasopharyngeal carcinoma cells in the absence of Epstein-Barr virus genome. J Biomed Sci *16*, 105.

Maschler, S., Gebeshuber, C.A., Wiedemann, E.M., Alacakaptan, M., Schreiber, M., Custic, I., and Beug, H. (2010). Annexin A1 attenuates EMT and metastatic potential in breast cancer. EMBO Mol Med *2*, 401-414.

Matushansky, I., Hernando, E., Socci, N.D., Mills, J.E., Matos, T.A., Edgar, M.A., Singer, S., Maki, R.G., and Cordon-Cardo, C. (2007). Derivation of sarcomas from mesenchymal stem cells via inactivation of the Wnt pathway. J Clin Invest *117*, 3248-3257.

Metsuyanim, S., Harari-Steinberg, O., Buzhor, E., Omer, D., Pode-Shakked, N., Ben-Hur, H., Halperin, R., Schneider, D., and Dekel, B. (2009). Expression of stem cell markers in the human fetal kidney. PLoS One *4*, e6709.
Natsuizaka, M., Ohashi, S., Wong, G.S., Ahmadi, A., Kalman, R.A., Budo, D., Klein-Szanto, A.J., Herlyn, M., Diehl, J.A., and Nakagawa, H. (2010). Insulin-like growth factor-binding protein-3 promotes transforming growth factor-{beta}1-mediated epithelial-to-mesenchymal transition and motility in transformed human esophageal cells. Carcinogenesis *31*, 1344-1353.
Nomura, D.K., Long, J.Z., Niessen, S., Hoover, H.S., Ng, S.W., and Cravatt, B.F. (2010). Monoacylglycerol lipase regulates a fatty acid network that promotes cancer pathogenesis. Cell *140*, 49-61.
Okada, H., Danoff, T.M., Kalluri, R., and Neilson, E.G. (1997). Early role of Fsp1 in epithelial-mesenchymal transformation. Am J Physiol *273*, F563-574.
Patel, P., West-Mays, J., Kolb, M., Rodrigues, J.C., Hoff, C.M., and Margetts, P.J. (2010). Platelet derived growth factor B and epithelial mesenchymal transition of peritoneal mesothelial cells. Matrix Biol *29*, 97-106.
Pebay, A., Bonder, C.S., and Pitson, S.M. (2007). Stem cell regulation by lysophospholipids. Prostaglandins Other Lipid Mediat *84*, 83-97.
Pelus, L.M., and Fukuda, S. (2006). Peripheral blood stem cell mobilization: the CXCR2 ligand GRObeta rapidly mobilizes hematopoietic stem cells with enhanced engraftment properties. Exp Hematol *34*, 1010-1020.
Polyak, K., and Weinberg, R.A. (2009). Transitions between epithelial and mesenchymal states: acquisition of malignant and stem cell traits. Nat Rev Cancer *9*, 265-273.
Ponzo, M.G., Lesurf, R., Petkiewicz, S., O'Malley, F.P., Pinnaduwage, D., Andrulis, I.L., Bull, S.B., Chughtai, N., Zuo, D., Souleimanova, M.*, et al.* (2009). Met induces mammary tumors with diverse histologies and is associated with poor outcome and human basal breast cancer. Proc Natl Acad Sci U S A *106*, 12903-12908.
Rak, J., Milsom, C., and Yu, J. (2008). Tissue factor in cancer. Curr Opin Hematol *15*, 522-528.
Reka, A.K., Kurapati, H., Narala, V.R., Bommer, G., Chen, J., Standiford, T.J., and Keshamouni, V.G. (2010). Peroxisome proliferator-activated receptor-{gamma} activation inhibits tumor metastasis by antagonizing Smad3-mediated epithelial-mesenchymal transition. Mol Cancer Ther *9*, 3221-3232.
Selmani, Z., Naji, A., Gaiffe, E., Obert, L., Tiberghien, P., Rouas-Freiss, N., Carosella, E.D., and Deschaseaux, F. (2009). HLA-G is a crucial immunosuppressive molecule secreted by adult human mesenchymal stem cells. Transplantation *87*, S62-66.
Sengupta, A., Arnett, J., Dunn, S., Williams, D.A., and Cancelas, J.A. (2010). Rac2 GTPase deficiency depletes BCR-ABL+ leukemic stem cells and progenitors in vivo. Blood *116*, 81-84.
Seo, D.C., Sung, J.M., Cho, H.J., Yi, H., Seo, K.H., Choi, I.S., Kim, D.K., Kim, J.S., El-Aty, A.A., and Shin, H.C. (2007). Gene expression profiling of cancer stem cell in human lung adenocarcinoma A549 cells. Mol Cancer *6*, 75.
Shao, M., Cao, L., Shen, C., Satpathy, M., Chelladurai, B., Bigsby, R.M., Nakshatri, H., and Matei, D. (2009). Epithelial-to-mesenchymal transition and ovarian tumor progression induced by tissue transglutaminase. Cancer Res *69*, 9192-9201.
Vuoriluoto, K., Haugen, H., Kiviluoto, S., Mpindi, J.P., Nevo, J., Gjerdrum, C., Tiron, C., Lorens, J.B., and Ivaska, J. (2010). Vimentin regulates EMT induction by Slug and oncogenic H-Ras and migration by governing Axl expression in breast cancer. Oncogene.
Yang, F., Huang, X.R., Chung, A.C., Hou, C.C., Lai, K.N., and Lan, H.Y. (2010). Essential role for Smad3 in angiotensin II-induced tubular epithelial-mesenchymal transition. J Pathol *221*, 390-401.
Yao, Z.X., Jogunoori, W., Choufani, S., Rashid, A., Blake, T., Yao, W., Kreishman, P., Amin, R., Sidawy, A.A., Evans, S.R.*, et al.* (2010). Epigenetic silencing of beta-spectrin, a TGF-beta signaling/scaffolding protein in a human cancer stem cell disorder: Beckwith-Wiedemann syndrome. J Biol Chem *285*, 36112-36120.

Yu, F., Hao, X., Zhao, H., Ge, C., Yao, M., Yang, S., and Li, J. (2010). Delta-like 1 contributes to cell growth by increasing the interferon-inducible protein 16 expression in hepatocellular carcinoma. Liver Int *30*, 703-714.